ELSEVIER

Journal of Photochemistry and Photobiology A: Chemistry 104 (1997) 69–76

Journal of PHOTOCHEMISTRY AND PHOTOBIOLOGY A:CHEMISTRY

Deactivation of excited 4′-dialkylamino-9-styrylacridines

U.-W. Grummt [a,*], E. Birckner [a], H. Lindauer [a], B. Beck [a], R. Rotomskis [b]

[a] *Institute of Physical Chemistry, Friedrich-Schiller-University Jena, Lessingstraße 10, D-07743 Jena, Germany*

[b] *Laser Research Centre, University of Vilnius, Vilnius, Lithuania*

Received 25 September 1996; accepted 2 January 1997

Abstract

The absorption and emission spectra and deactivation of excited styrylacridines are determined by the flexibility and charge transfer properties of the donor–acceptor chromophore system. The fluorescence and excitation spectra, as well as the kinetics, vary with the excitation and emission wavelength respectively. Principal component analysis (PCA) and global analysis of the spectra and kinetics of the E isomers reveal at least two absorbing and two emitting components in fluid solution at room temperature as well as in a frozen matrix. At 77 K, the fluorescence of the Z isomer is also observed. The $S_n \leftarrow S_1$ transition of the Z isomer is the only transient detectable from picosecond time-resolved absorption experiments in solution. The main competing deactivation channels of the S_1 state are E→Z isomerization, charge transfer-induced internal conversion and fluorescence. © 1997 Elsevier Science S.A.

Keywords: Aminostyrylacridine; Fluorescence kinetics; Photoisomerization

1. Introduction

Unsubstituted 4′-dialkylamino-9-styrylacridines (SAs) were investigated initially by Zanker and Reichel [1]. Later, substituted SAs were studied with respect to their proposed application as UV stabilizers for polymeric materials [2] and in solar energy research [3]. We have recently reported the synthesis and visible spectra of acidochromic SAs and several other types of dye absorbing in the red or near-IR spectral region which had originally been designed as pH-sensitive sensitizers [4–6]. Chemical engineering was successful in obtaining the absorption of the protonated form in the desired region, together with a pK_a value near the physiological range and chemical stability. However, it was not possible to accomplish sufficiently large intersystem crossing rates by heavy atom substitution.

SAs are aza analogues of diarylethylenes. In comparison with 9-styrylanthracenes [7–10], the aza substitution changes the donor–acceptor properties of the molecules and causes pH sensitivity. For the aza analogues of diarylethylenes, considerably less experimental data and theoretical results are available in the literature [11].

We wished to elucidate quantitatively the relaxation behaviour of the first excited state. Further motivation for the investigation of the photophysics and photochemistry of the title compounds originated from their excellent qualification as chemical sensor dyes [12–14].

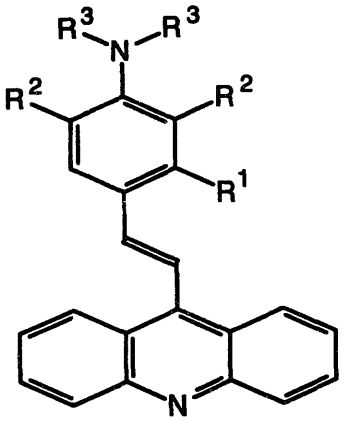

Nr.	R^1	R^2	R^3
1	H	H	C_2H_5
2	OH	H	C_2H_5
3	OC_2H_5	H	C_2H_5
4	$OC_{18}H_{37}$	H	C_2H_5
5	H	$(CH_2)_3$	

Scheme 1.

For this study, we selected the compounds shown in Scheme 1. The variation of the chemical structure involves

* Corresponding author.

PII S1010-6030(97)00006-3

steric fixation of the amino substituent in order to determine whether rotation or pyramidalization of this group plays a role in the deactivation process. A substituent in the 2'-position should remove the degeneracy of the rotamers.

2. Experimental details

The synthesis of the compounds has been described in Ref. [4]. The purity of all compounds was thoroughly confirmed by thin layer chromatography using different solvents and solvent mixtures. In order to avoid the establishment of photostationary equilibria under the influence of daylight, all solutions were prepared in the dark.

The solvents ethanol (EtOH), toluene and methylcyclohexane (MCH) from Aldrich were of spectrophotometric grade.

Photokinetic experiments were performed with an M400 spectrophotometer (Carl Zeiss, Jena). Stationary and time-resolved emission spectra were recorded with an LS-50B luminescence spectrometer (Perkin–Elmer) and a time-correlated single-photon counting spectrometer CD900 (Edinburgh Instruments). The picosecond time-resolved experiments were performed using a home-built spectrometer described in Ref. [15].

Fluorescence quantum yields at room temperature and at 77 K were determined from the integrated corrected fluorescence spectra of dilute solutions ($(1–5)\times10^{-5}$ M) relative to the yields of rhodamine 6G in EtOH ($\Phi_f=0.95$ at 293 K and $\Phi_f=1$ at 77 K). The fluorescence measurements at 77 K were carried out in silica tubes of 2 mm inner diameter. Absorbance changes with temperature were measured separately. The refractive index at 77 K was corrected by a factor of $[n(77\text{ K})/n(293\text{ K})]^2=1.08$ [16].

In order to calculate the fluorescence lifetimes from the decay curves and the time-resolved spectra from the time-resolved emission scans, the LEVEL 1 (up to four-exponential fit) and LEVEL 2 (global analysis of up to 100 decay curves) analysis packages implemented in the Edinburgh Instruments software were used.

The experimental errors of the fluorescence quantum yields are ±0.001 at room temperature and ±0.1 at 77 K. The error of the measured lifetimes is ±0.1 ns.

Principal component analysis (PCA) was performed without any data preprocessing using the standard algorithms described in Ref. [17].

The quantum chemical calculations were performed using the AM1 hamiltonian [18] within the semiempirical program package VAMP5.6 [19].

3. Results

3.1. Stationary absorption and emission

The absorption spectra of the E isomers are characterized by a broad, unstructured long-wavelength band in the visible

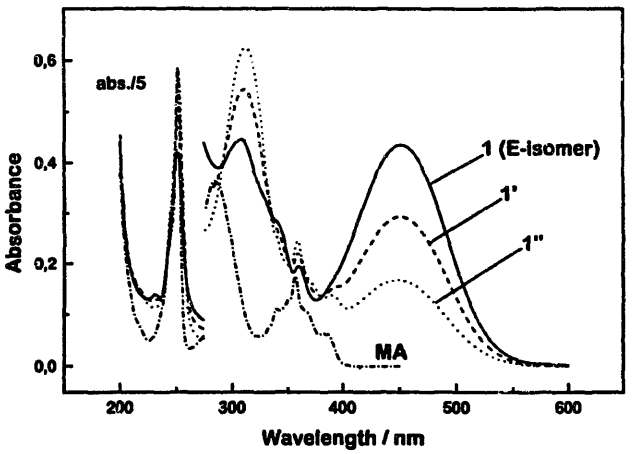

Fig. 1. Absorption spectra of unirradiated (E isomer) and irradiated ($\lambda'=436$ nm) Z-enriched (1', 1") solutions of **1** and 9-methylacridine (MA) in ethanol at 293 K.

spectral region and well-structured bands in the UV. The long-wavelength bands show a pronounced positive solvatochromism and strong bathochromic and hyperchromic effects on cooling to the glass point of the solvent [20]. In contrast with this observation, the UV bands remain essentially unchanged.

All compounds show efficient photoisomerization. Fig. 1 shows the absorption spectra of the pure E form of **1** and of Z-enriched solutions in EtOH obtained by subsequent irradiation with $\lambda_{exc}=436$ nm. The spectrum of the Z isomer calculated according to Fischer's method [21] is given in Ref. [20]. The quantum yields of E→Z and Z→E photoisomerizations are given in Table 1, together with the fluorescence quantum yields, lifetimes, positions of the absorption and fluorescence maxima and their molar absorptivities.

The thermal reverse (Z→E) reaction follows first-order kinetics in EtOH or toluene solution. In toluene, for instance, values of 42 kJ mol^{-1} and -194 J mol^{-1} K^{-1} are determined for the activation enthalpy and entropy of **1** by fitting the experimental rate constants in the temperature range 313–378 K to the Eyring equation. However, systematic deviations of the experimental rate constants from the Eyring equation are observed. Arrhenius plots are convex from above which indicates a consecutive reaction [22]. The rate constants are very sensitive to acidic impurities. On handling the solutions under laboratory conditions, sufficient amounts of moisture and carbon dioxide are shown to have a drastic influence on the kinetics. Acid catalysis of the thermal isomerization has also been observed by Bastianelli et al. [3].

The activation barriers obtained by transition state calculations on this Z→E reaction are 238 kJ mol^{-1} and 84 kJ mol^{-1} for the base and protonated form of **1** (unsubstituted amino group) respectively. Although the numerical values are unreasonably high, the dramatic reduction of the activation energy by protonation is correctly predicted. The same qualitative result is obtained with UHF calculations. Saddle point calculations for the excited state E→Z isomerization yield 42 kJ mol^{-1} above the S_1 minimum for the E form. The

Table 1
Spectroscopic data, quantum yields of fluorescence and E⇔Z isomerization and mean fluorescence decay time of SAs at room temperature

Compound	Solvent	λ_a (nm)	ϵ ($M^{-1}cm^{-1}$)	λ_f (nm)	$\Delta\nu_{af}$ (cm^{-1})	Φ_f	$\langle\tau\rangle$ (ns)[a]	Φ^b_{EZ}	Φ^b_{ZE}
1	MCH	418	20 200	580	6700	0.0009	–	0.28	0.61
	EtOH	450	16 400	650	6850	0.0044	0.27		
2	MCH	423	–	568	6000	<0.001	–	–	–
	EtOH	472	16 100	642	5600	0.0033	0.18		
3	MCH	426	20 600	590	6550	0.0005	–	0.37	0.53
	EtOH	464	16 600	650	6170	0.0037	0.12		
4	MCH	428	14 700	565	5660	0.0009	–	0.27	0.74
	EtOH	464	12 600	650	6170	0.0043			
5	MCH	432	16 500	570	5600	0.0010	–	0.31	1.04
	EtOH	469	13 470	670	6400	0.0053	0.23		

[a]Calculated from a biexponential fit $I(t)=B_1\exp(-t/\tau_1)+B_2\exp(-t/\tau_2)$ and $\langle\tau\rangle=(B_1\tau_1+B_2\tau_2)/(B_1+B_2)$.
[b]Solvent, toluene.

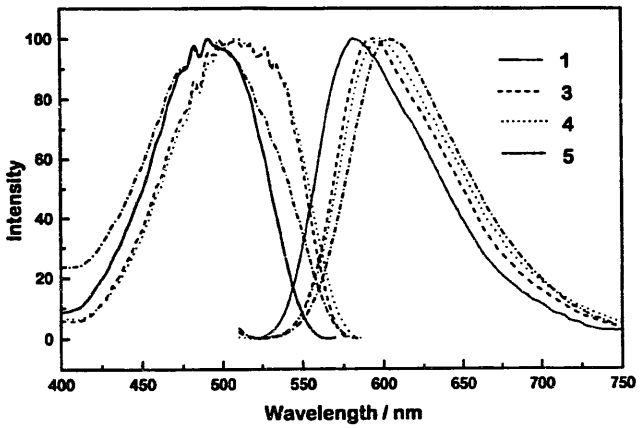

Fig. 2. Corrected normalized fluorescence excitation (λ_f=600 nm) and emission (λ_{ex}=500 nm) spectra of SAs in ethanol ((1–2)×10^{-5} M) at 77 K.

torsion angle of the central double bond is 40°, whereas the remaining two torsion angles of the chain are close to zero.

The fluorescence of all compounds (E isomers) in solution is weak at room temperature (see Table 1). The emission spectra are unstructured and depend on the excitation wavelength; the excitation spectra depend on the emission wavelength chosen. In both cases, the observations are independent of the Z isomer concentration. Therefore we conclude that the Z isomers are non-fluorescent at room temperature.

Aggregation has been excluded as a conceivable reason for the spectral effects observed. The band shapes of the absorption spectra and the molar absorptivities are independent of the concentration within a wide range. The validity of Beer's law has been proven with **1** and **4** in EtOH at room temperature in the concentration range 5×10^{-7}–5×10^{-4} M.

The decay curves are non-exponential. Biexponential fits yield decay constants of 100–200 ps and 3–4 ns for the main (95% of the emission) and secondary components respectively.

On cooling from room temperature to 77 K, the fluorescence intensity increases by two orders of magnitude. The temperature dependence of the apparent fluorescence quantum yield of **1** in EtOH in the temperature range 293–163 K fits well with the equation

$$\ln\left(\frac{1}{\Phi_f}-1-\frac{k^0_{nr}}{k_f}\right)=\ln\frac{k^1_{nr}}{k_f}-\frac{\Delta E}{R}\frac{1}{T}$$

where k^0_{nr} and $k^1_{nr}\exp(-\Delta E/RT)$ are the temperature-independent and temperature-dependent non-radiative rate constants respectively. The temperature dependence of the radiative rate constant k_f has been neglected in this fit. The parameters found are $k^0_{nr}/k_f=9$, $k^1_{nr}/k_f=1.3\times10^5$ and E=15.4 kJ mol^{-1}.

Table 2
Absorption and fluorescence of SAs in ethanol at 77 K

Compound	λ_a (nm)	λ_c (nm)[b]	λ_f (nm)[a]	Φ^a_f	$\langle\tau\rangle$ (ns)[a,b,c]	$\Phi_f/\langle\tau\rangle$ ($10^8\,s^{-1}$)	ϵ_{max} ($M^{-1}cm^{-1}$)	k_f(SB) ($10^8\,s^{-1}$)[d]
1	500	495	583	0.5_3	3.7	1.4	24300	1.1
2	–	515	596	0.5_4	3.8	1.4	–	–
3	509	512	595	0.5_4	4.6	1.2	22800	1.1
4	516	510	598	0.3_2	–	–	17900	0.81
5	503	494	605	0.4_7	4.3	1.1	19000	0.92

[a]λ_{ex}=500 nm.
[b]λ_{em}=600 nm.
[c]Calculated from a biexponential fit $I(t)=B_1\exp(-t/\tau_1)+B_2\exp(-t/\tau_2)$ and $\langle\tau\rangle=(B_1\tau_1+B_2\tau_2)/(B_1+B_2)$.
[d]Calculated from the absorption and corrected fluorescence spectra according to the Strickler–Berg formula.

Fig. 2 shows the fluorescence emission and excitation spectra of the different SAs in EtOH at 77 K. Comparison of the absorption and excitation spectra ($\lambda_{em}=600$ nm) gives only small deviations in the band shapes. Additional absorption and fluorescence data are given in Table 2.

The excitation/emission wavelength dependence of the fluorescence spectra and of the kinetics is also observed at 77 K. For most of the excitation/emission wavelength combinations, the decay curves are at least biexponential. Taking these results into account, the values of the quantum yields and lifetimes in Table 2 must be regarded as weighted means.

In order to investigate the nature of the excited state and the character of the emitting components, the excitation wavelength dependence of the fluorescence spectra and the excitation/emission wavelength dependence of the fluorescence kinetics, particularly at 77 K, in EtOH and MCH were studied in more detail by PCA and global analysis. Fig. 3 shows a series of fluorescence spectra of **2** (E isomer) in EtOH at 77 K, excited at different wavelengths between 440 and 570 nm. The observed red shift of the fluorescence maximum with increasing excitation wavelength is typical of all compounds studied. This is definitely not caused by inner filter effects. The absorbance of the solutions at 77 K in the overlap region is less than 0.1, resulting in a re-absorption of fluorescence at 596 nm (fluorescence maximum of **2**) of less than 2%.

Differences between differently substituted compounds become obvious if they are excited at the long-wavelength edge of the absorption band near 500 nm. The fluorescence spectra of the compounds containing a substituent $R^1 \neq H$ show a somewhat more pronounced shoulder at the long-wavelength edge.

The results of PCA obtained from the measurement of a series of fluorescence spectra of **1**, **2** and **3** in EtOH (E isomer) at 77 K are given in Table 3. As can be seen from the PCA results, two components are calculated for the E isomers of the differently substituted SAs, excited at the main region of the long-wavelength absorption band, outside the overlap region of absorption and fluorescence (see Fig. 3).

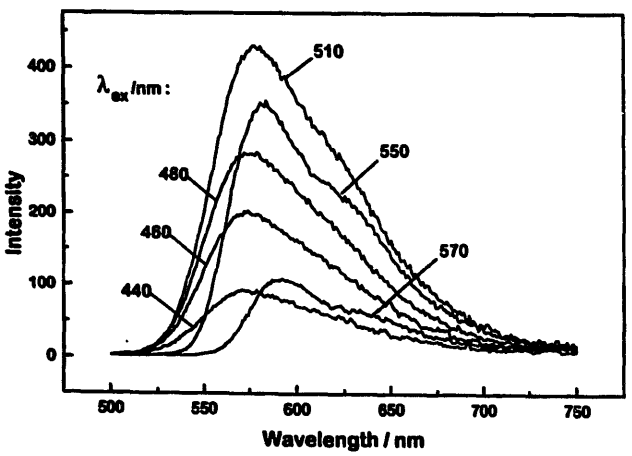

Fig. 3. Fluorescence spectra of **2** (1.3×10^{-5} M) in ethanol at 77 K: excitation wavelength dependence.

Table 3
Results of PCA of the fluorescence of **1**, **2** and **3** in ethanol at 77 K

Compound	Excitation range (nm) (number of spectra)	Number of significant eigenvectors	Variance (%)
1	430–550 (25)	4	99.99
	430–520 (19)	2	99.98
2	440–570 (14)	3	99.97
	440–530 (10)	2	99.97
3	440–570 (14)	4	99.99
	440–530 (10)	2	99.99

Extension of excitation to the long-wavelength absorption edge increases the number of components to three and four respectively. We were able to exclude impurities and re-absorption effects, as well as luminescence originating from the Z isomer, as the source of these observations.

Polarization measurements were performed in EtOH at 77 K. The results are sensitive to the glassy quality of the frozen sample. For good glasses, the fluorescence anisotropy has been found to be essentially constant and close to the theoretical value over the entire emission and long-wavelength absorption region (**1**, $r=0.36\pm0.01$; **2**, $r=0.35\pm0.01$). On excitation into the short-wavelength wing of the lowest absorption band, a decrease in anisotropy is found towards longer emission wavelengths.

3.2. *Time-resolved emission*

The fluorescence kinetics were studied in more detail at 77 K in order to avoid further complications in the fluorescence decay due to solvation dynamics. Monoexponential fits of a series of 16 decay curves of **1** (E isomer) in EtOH, excited at the long-wavelength absorption maximum (500 nm) and measured in the region of the fluorescence spectrum between 550 and 700 nm, result in a systematic increase in the lifetimes from 3.83 ns to 4.04 ns. The global fit of all the decay curves yields a consistent biexponential description with lifetimes of 3.1 and 4.3 ns. The existence of two emitting species is in good agreement with the results of PCA in the main absorption region. In contrast, the decay curves, excited at the long-wavelength absorption edge (550 nm) and calculated with the global fitting procedure, are essentially monoexponential (3.91 ns). A consistent global fit of the decay curves, excited along the whole absorption spectrum, was not successful. Similar results were obtained with the other SAs.

A different decay behaviour was found in the non-polar solvent MCH at 77 K. The global fits of a series of decay curves of **1**, **3** and **5**, excited at the absorption maxima and measured along the fluorescence spectra, give three emitting components. The time constants and integrated decay-associated spectra from the global analysis of the time-resolved fluorescence measurements are given in Table 4 and Fig. 4. The component showing the smallest Stokes shift is always that with the shortest lifetime and the longest lived component is always associated with the largest Stokes shift.

Table 4
Decay times and integrated decay-associated spectra: results of global analyses

Compound	Solvent	Component i	τ_i (ns)	$\lambda_{n,i}$ (nm)	$\Phi_{n,i}$
1	EtOH	1	3.1	570	0.36
		2	4.3	590	0.64
	MCH	1	1.8	545	0.30
		2	4.0	560	0.60
		3	13	580	0.10
3	EtOH	1	3.1	–	0.20
		2	4.2	–	0.80
	MCH	1	1.1	540	0.16
		2	3.1	560	0.63
		3	19	610	0.21
5	EtOH	1	3.5	600	0.28
		2	4.7	625	0.72
	MCH	1	1.6	570	0.36
		2	3.2	560	0.43
		3	6.7	570	0.21

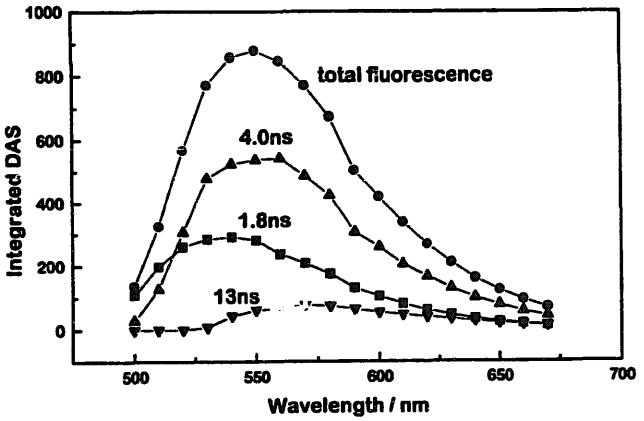

Fig. 4. Integrated decay-associated spectra (DAS) of 1 in methylcyclohexane at 77 K.

In addition to the fluorescence measurements of the E isomer of 1, we recorded the fluorescence spectra and kinetics of irradiated probes containing both E and Z isomers. At 77 K in EtOH, the fluorescence spectrum (i.e. the superposition of the spectra of the E and Z isomers) appears somewhat red shifted; the number of components calculated by PCA increases by one compared with the pure E isomer (Table 3). Subtracting the fluorescence spectrum of the E form from that of the Z-enriched mixture allows an estimation to be made of the fluorescence maximum of the Z isomer: 630 nm.

The fluorescence decay time of the Z isomer is 10.2 ± 0.7 ns, very different from that of the E isomer.

3.3. Time-resolved absorption

Picosecond time-resolved absorption measurements were performed with 1 and in more detail with 2 in acidic, neutral and alkaline solutions. Irrespective of the pH, the transient absorption kinetics become stationary within 500 ps. All absorption changes persisting after this time are due to $E \rightarrow Z$ isomerization. Taking into account the considerably smaller dynamic range and accuracy of the picosecond time-resolved absorption compared with the single-photon counting emission experiments, all decays can be described by a single exponential. The $S_n \leftarrow S_1$ absorption is the only transient observable. Table 5 shows the decay times of the transient absorption or depletion of 2 measured at different wavelengths and pH values in EtOH. Examples of the transient absorption spectra and corresponding decay curves are given in Fig. 5 and Fig. 6.

4. Discussion

4.1. Absorption spectra

The absorption spectra of the SAs may be interpreted as the superposition of a long-wavelength charge transfer tran-

Table 5
Lifetimes (ps) of transient absorption and depletion signals of 2

pH	λ_{probe} (nm) 400	450	505	600	700	800
4.2	72 ± 7	106 ± 36	–	82 ± 2	70 ± 2	108 ± 22
6.7	p.w.l.[a]	59 ± 37	–	83 ± 10	78 ± 11	274 ± 494
13	p.w.l.	103 ± 43	67 ± 17	59 ± 6	p.w.l.	p.w.l.

[a] p.w.l., pulse width limited.

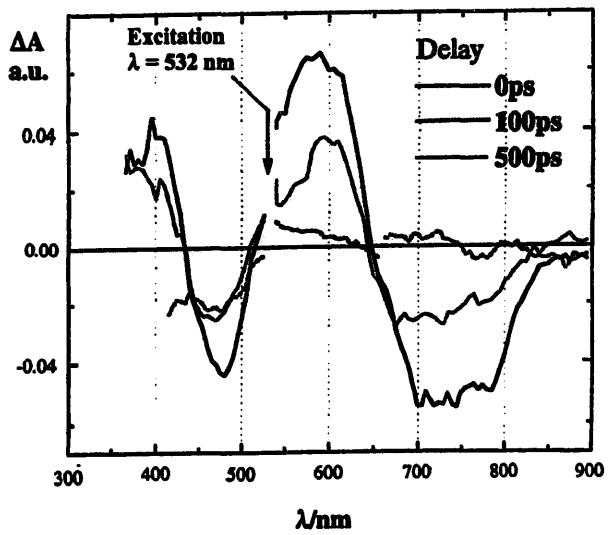

Fig. 5. Transient absorption spectra of 2 in ethanol (1.47×10^{-4} M, pH 6.7). The excitation pulse width was 30 ps.

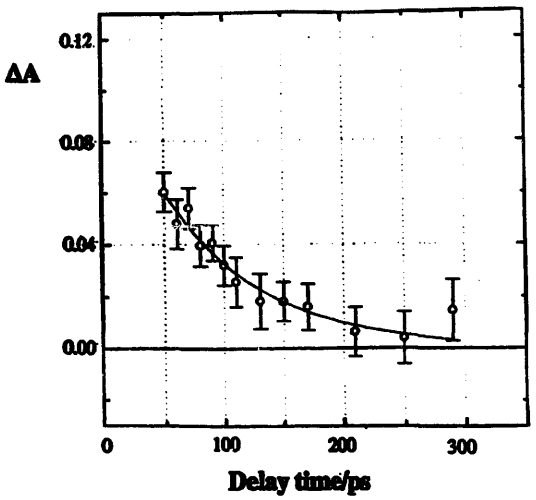

Fig. 6. Decay of the excited state absorption of 2 recorded at 600 nm.

sition and transitions to locally excited states of the subchromophores. This becomes particularly obvious from a comparison with the absorption spectrum of 9-methylacridine (MA) (cf. Fig. 1). MA shows an intense band at 251 nm and unstructured and vibrationally structured transitions at 300 and 356 nm respectively. This is also the case in the spectra of the SAs. The longest wavelength electronic transition of the SAs shows marked bathochromic and hypsochromic effects with increasing solvent polarity as expected for charge transfer transitions, as can be seen from the data in Table 1. Long-wavelength charge transfer transitions have been observed for various push-pull substituted diarylethylenes. The stronger acceptor 9-acridyl causes a more pronounced bathochromic shift of the charge transfer transition compared with 4-dimethylaminostyryl-9-anthracenes [10]. This is also the reason for the absence of a long-wavelength charge transfer absorption band for 4-nitrostyryl-9-acridine [2] compared with 4-nitrostyryl-9-anthracenes [10].

The molar absorptivities and positions of the absorption maxima are only weakly affected by the substituents R^1, R^2 and R^3. Compared with MA, the intensity of the locally excited transition is significantly lower than that of the charge transfer transition. Sterically hindered SAs (Z isomer) exhibit considerably weaker charge transfer bands and comparatively more intense local transitions. As observed with other substituted SAs, the absorption of the Z isomer is less determined by new transitions than by an altered intensity ratio between the local and charge transfer transitions.

4.2. Photoisomerization

Torsion around the central double bond leading to the Z isomer is an efficient deactivation channel of excited SAs. The quantum yields of about 0.3 (see Table 1) are of the same order of magnitude as observed for comparable aryl ethylenes [23] and 4′-dimethyl-aminostyryl-9-anthracene [10]. There is no systematic dependence on the substituent pattern. Population of the triplet state is not observed. Triplet–triplet absorption is not detected by conventional flash photolysis with microsecond time resolution. Furthermore, singlet oxygen generation is not detected on prolonged irradiation [4] and no phosphorescence is detected in a frozen EtOH matrix at 77 K. The picosecond time-resolved absorption experiments do not reveal any transient other than the S_1 state. These experimental findings are in favour of a singlet pathway of isomerization, which was also proposed for the 9-styrylanthracenes [9,10].

4.3. Fluorescence and AM1 calculations

The position and form of the fluorescence spectra, as well as the small quantum yields and short lifetimes, indicate the predominance of radiationless relaxation of the S_1 state. In the non-polar solvent MCH, the Stokes shift is surprisingly large and hardly increases in EtOH. This means that a significant geometrical relaxation of the excited state must be taken into consideration, as well as solvation effects in both solvents.

When discussing the dependence of the emission spectra on the excitation wavelength in more detail, it should be kept in mind that no fluorescence of the Z isomer is obtained at room temperature, as observed for 4′-substituted 9-styrylanthracenes [7,9].

There are many examples of excitation wavelength-dependent fluorescence spectra and emission wavelength-dependent excitation spectra in diarylethylenes and their heteroaromatic analogues [11]. In all these cases, distinct rotamers exist. For instance, the existence of two rotamers has been predicted from quantum chemical calculations for 1-styrylanthracene and 2-styrylanthracene. Fluorescence investigations reveal two rotamers only for 2-styrylanthracene and not for the 1-isomer. This was explained by the calculated unfavourable high energy difference between the two rotamers. As expected, no rotamers were found experimentally for 9-styrylanthracene [24].

Due to the local C_2 symmetry of the aromatic moieties, at least in compounds **1** and **5**, no distinguishable rotamers exist if the corresponding formal single bonds are considered sep-

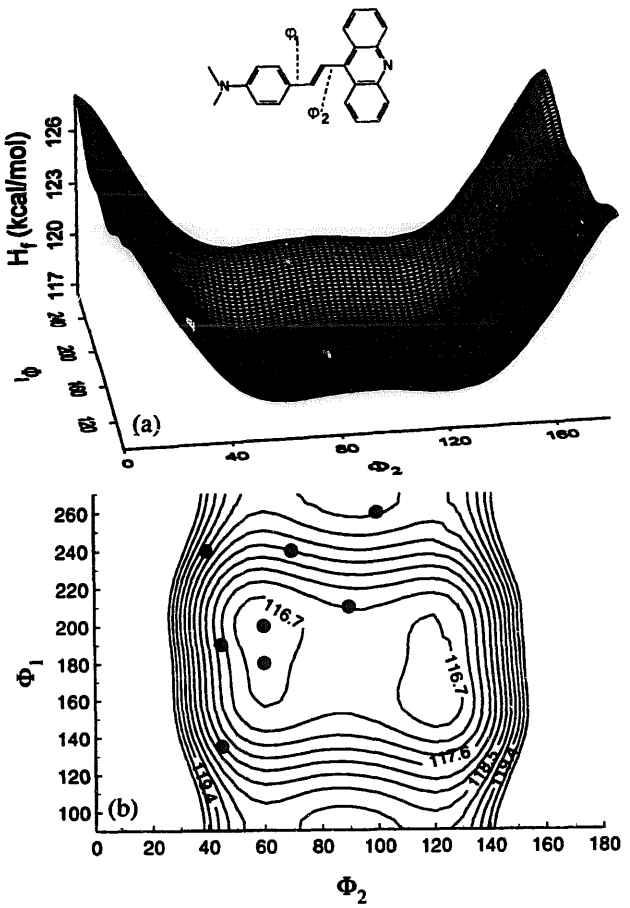

Fig. 7. Calculated ground state energy surface of diethylamino-styrylacridine (**1**). Φ_1 describes the rotation of the diethylaminophenyl ring around the single bond to the central ethylene group. Φ_2 describes the rotation of the rest of acridine in the same way. (a) Three-dimensional plot of the energy surface. (b) Contour plot of the central part of the surface including all points for which the S_1 structures were optimized.

arately. However, there are two possibilities of combining two arrangements of both aromatic rings twisted either in the same or opposite directions with respect to the plane of the ethylene moiety which will result in two different rotameric forms. As deduced from temperature-dependent ^1H nuclear magnetic resonance (NMR) spectroscopy [20], the aminophenyl ring rotates freely at room temperature and the rotation is not frozen even at 150 K in tetrahydrofuran within the time scale of a 400 MHz spectrometer. AM1 calculations predict a rotational barrier of less than 8.5 kJ mol^{-1}, which is in qualitative agreement with experiment. Due to the nearly free rotation, the degeneracy of the two rotameric positions of the aminophenyl ring is not removed by substitution as long as the temperature is not too low.

The bond orders of the formal single bonds connecting the aromatic rings with the ethylene moiety increase in the excited state. This can be predicted qualitatively by analogy using the Imamura–Hoffmann rules [25] and has been confirmed quantitatively by the calculations.

Semiempirical calculations were performed for diethylamino-styrylacridine **1**. Fig. 7 shows a three-dimensional and contour plot of the calculated ground state energy surface along the torsion angles of the aniline and the acridine rings. Starting with the ground state geometries marked in Fig. 7(b), we also optimized the S_1 excited state. For the resulting structures, the Franck–Condon transition energies and oscillator strengths were calculated.

As mentioned before, the main difference between the ground state and excited state geometries is that the torsion angles of the aromatic rings and the central ethylene group are much smaller for the excited states. For the eight optimized S_1 geometries, we found heats of formation of between 186.6 and 187.4 kcal mol^{-1}. The calculated transition energies are between 2.73 eV (453 nm) and 2.87 eV (432 nm). At present, the structures obtained can be divided into three minima at the S_1 energy surface. These minima have nearly the same heats of formation and oscillator strengths, but differ slightly in the calculated emission wavelengths. Further calculations, including solvent simulation, are necessary to obtain a sophisticated explanation of the experimental findings.

In solution, we always excite a large distribution of rotational or librational excited molecules. Variation of the excitation wavelength produces different primary populations of Franck–Condon states. Relaxation of librationally excited states corresponds to large-amplitude motions and is expected to be comparatively slow. Taking into account the very short fluorescence lifetimes observed, we may tentatively explain the effects by a contribution of hot fluorescence which varies with the excitation wavelength.

In contrast with the majority of diarylethylenes, including the hetero analogues investigated in Ref. [11], the missing vibrational structure of the longest wavelength transition and the very small fluorescence quantum yields render data analysis considerably more complicated. Therefore we extended the fluorescence decay analysis to 77 K. In a frozen matrix at 77 K, we expect to obtain a frozen non-equilibrium distribution with respect to the torsion angles of the single bonds, which represents the equilibrium state near the glassy point.

The reduced Stokes shift of 3000 cm^{-1} and the increase in the fluorescence quantum yield by two orders of magnitude at 77 K indicate a diminished geometric relaxation and a significantly reduced efficacy of non-radiative deactivation which is, however, still as efficient as 0.5. E→Z isomerization is not found in a frozen EtOH matrix at 77 K. PCA and global analysis of the fluorescence spectra and kinetics reveal the existence of at least two fluorescent components independent of the substituent. Three components with significantly different decay constants are detected in the non-polar solvent MCH. Obviously, substitution at the 2-position of the aminophenyl ring does not produce a discernible removal of the degeneracy of the rotameric forms.

Our experimental findings cannot be explained solely with the assumption of two rotamers. Presumably, in the frozen matrix, in addition to the distribution of torsion angles, various solvation sites exist which give rise to different spectral and deactivation behaviour. This would explain the increased number of components detected by PCA for long-wavelength

excitation (Table 3). On the other hand, the satisfactory coincidence of the radiative fluorescence rate constants, obtained from the lifetime and yield data and by the Strickler–Berg formula, is in favour of small differences in the deactivation behaviour between different torsion geometries or solvation sites (Table 2). The same conclusion could be drawn from the practically constant fluorescence anisotropy over the longest wavelength absorption and fluorescence bands.

The sum of our results cannot be interpreted in terms of the twisted intramolecular charge transfer (TICT) concept [26] or by a solvent-induced pseudo-Jahn–Teller effect of the excited state [27], which is underlined by the following arguments. The julolidine derivative (**5**) does not show any significant differences in comparison with the sterically unfixed amino compounds. No distinct dual luminescence is observed, and no rise time is obtained in the fluorescence kinetics. The dependence of the excitation and fluorescence spectra on the emission and excitation wavelengths respectively is observed in polar and non-polar solvents. No perpendicular minima are found in the quantum chemical calculations of the excited state.

A reasonable assignment of the principal components to absorbing and emitting species defined according to their geometry and solvation site seems impossible at present.

The origin of the transient depletion signal observed above 800 nm is not yet fully understood. The most probable explanation involves the (stimulated) fluorescence of protonated species. A very weak fluorescence is observed peaking at 730 nm under stationary conditions with a laser Raman spectrometer.

Due to the short lifetime, especially of protonated SAs, it is unlikely that useful sensitizers will be prepared from this type of dye unless stiff derivatives become synthetically available. On the other hand, the very rapid deactivation guarantees high photostability which is an important prerequisite for sensor applications.

Acknowledgements

This work was supported by the Deutsche Forschungsgemeinschaft under project Di 481/1-2, which is gratefully acknowledged. U.-W.G. thanks the Fonds der Chemischen Industrie for financial support.

References

[1] V. Zanker, A. Reichel, Ber. Bunsenges. Phys. Chem. 64 (1960) 431.
[2] A.P. Kucherenko, S.G. Potashnikova, S.S. Radkova, S.N. Baranov, A.K. Sheinkman and N.V. Volbushko, Khimiya Geterosikl. Soedin. 9 (1974) 1257.
[3] C. Bastianelli, V. Caia, G. Cum, R. Gallo, V. Mancini, J. Chem. Soc., Perkin Trans. 2 (1991) 679.
[4] H. Lindauer, P. Czerney, U.-W. Grummt, J. Prakt. Chem. 336 (1994) 521.
[5] H. Lindauer, P. Czerney, U.-W. Grummt, J. Inf. Rec. Mater. 21 (1994) 619.
[6] H. Lindauer, P. Czerney, U.-W. Grummt, J. Prakt. Chem. 337 (1995) 216.
[7] K. Sandros, H.-D. Becker, J. Photochem. 39 (1987) 301.
[8] H.-D. Becker, Adv. Photochem. 15 (1989) 193. O. Axelsson, Ph.D. Thesis, University of Göteborg, 1989.
[9] H. Görner, J. Photochem. Photobiol. A: Chem. 43 (1988) 263.
[10] L. Sun, H. Görner, J. Phys. Chem. 97 (1993) 11 186.
[11] U. Mazzucato, F. Momicchioli, Chem. Rev. 91 (1991) 1679.
[12] H. Lindauer, P. Czerney, G.J. Mohr, U.-W. Grummt, Dyes Pigm. 26 (1994) 229.
[13] H. Lehmann, G. Schwotzer, P. Czerney, G.J. Mohr, Sensors Actuators B 29 (1995) 392.
[14] R. Koncki, G.-J. Mohr, O.S. Wolfbeis, Biosens. Bioelectr. 10 (1995) 653.
[15] R. Danelius, A. Piskarskas, V. Sirukaitis, Sov. Quantum Electron. 12 (1982) 1626.
[16] W. Regenstein, Exp. Tech. Phys. 39 (1991) 257.
[17] E.R. Malinowski, Factor Analysis in Chemistry, Wiley, New York, 1991.
[18] M.J.S. Dewar, E.G. Zoebisch, E.F. Hersley, J.J.P. Stewart, J. Am. Chem. Soc. 107 (1985) 3902.
[19] G. Rauhut, A. Alex, J. Chandrasekhar, T. Steinke, W. Sauer, B. Beck, M. Hutter, P. Gedeck, T. Clark, VAMP5.6, Oxford Molecular Ltd., Magdalen Centre, Oxford Science Park, Sandford-on-Thames, Oxford, OX4 4GA, UK.
[20] U.-W. Grummt, E. Birckner, P. Czerney, J. Inf. Rec. Mater. 22 (1996) 533.
[21] E. Fischer, J. Phys. Chem. 71 (1967) 3704.
[22] R. Schmid, V.N. Sapunov, Non-Formal Kinetics, VCH, Weinheim, 1982.
[23] H. Görner, Adv. Photochem. 19 (1995) 1.
[24] G. Bartocci, G. Mazzucato, I. Baraldi, E. Fischer, J. Mol. Struct. 193 (1989) 173.
[25] A. Imamura, R. Hoffmann, J. Am. Chem. Soc. 90 (1968) 5379.
[26] W. Rettig, in J. Mattay (ed.), Topics in Current Chemistry, vol. 169, Springer Verlag Berlin, 1994, p. 253.
[27] K.A. Zachariasse, T.v.d. Haar, A. Hebecker, U. Leinhos, W. Kühnle, Pure Appl. Chem. 65 (1993) 1745.